

# Metazoan zooplankton in the Bay of Biscay: 16 years of individual sizes and abundances combining ZooScan and ZooCAM imaging systems.

## Authors

Grandremy Nina<sup>1\*</sup>, Bourriau Paul<sup>1</sup>, Daché Edwin<sup>2</sup>, Danielou Marie-Madeleine<sup>3</sup>, Doray Mathieu<sup>1</sup>, Dupuy Christine<sup>4</sup>, Forest Bertrand<sup>5</sup>, Jalabert Laetitia<sup>6</sup>, Huret Martin<sup>7</sup>, Le Mestre Sophie<sup>7</sup>, Nowaczyk Antoine<sup>8</sup>, Petitgas Pierre<sup>9</sup>, Pineau Philippe<sup>4</sup>, Rouxel Justin<sup>10</sup>, Tardivel Morgan<sup>10</sup>, Romagnan Jean-Baptiste<sup>1\*</sup>.

## Correspondence

[grandremy.n@gmail.com](mailto:grandremy.n@gmail.com), [jean.baptiste.romagnan@ifremer.fr](mailto:jean.baptiste.romagnan@ifremer.fr)

## Affiliations

<sup>1</sup> DECOD (Ecosystem Dynamics and Sustainability), IFREMER, INRAE, Institut Agro, Nantes, Centre Atlantique - Rue de l'Île d'Yeu - BP 21105 - 44311 Nantes Cedex 03, France.

<sup>2</sup> Unité Biologie et Ecologie des Ecosystèmes marins Profonds, Laboratoire Environnement Profond, Ifremer Centre Bretagne - ZI de la Pointe du Diable - CS 10070 - 29280 Plouzané, France.

<sup>3</sup> Unité DYNECO-PELAGOS, Laboratoire d'Ecologie Pélagique, Ifremer Centre Bretagne - ZI de la Pointe du Diable - CS 10070 - 29280 Plouzané, France.

<sup>4</sup> BIOFEEL, UMRi LIENSs, La Rochelle University / CNRS, 2, rue Olympe de Gouges, 17000 La Rochelle, France.

<sup>5</sup> Laboratoire Hydrodynamique Marine, Unité RDT, Ifremer Centre Bretagne - ZI de la Pointe du Diable - CS 10070 - 29280 Plouzané, France.

<sup>6</sup> Sorbonne Université, Institut de la Mer de Villefranche, 06230 Villefranche-sur-mer, France.

<sup>7</sup> DECOD (Ecosystem Dynamics and Sustainability), IFREMER, INRAE, Institut Agro, Centre Bretagne - ZI de la Pointe du Diable - CS 10070 - 29280 Plouzané, France.

<sup>8</sup> UMR CNRS 5805 EPOC – OASU, Station Marine d'Arcachon, Université de Bordeaux, 2 Rue du Professeur Jolyet, 33120 Arcachon, France.

<sup>9</sup> Département Ressources Biologiques et Environnement, Ifremer Centre Atlantique - Rue de l'Île d'Yeu - BP 21105 - 44311 Nantes Cedex 03, France.

<sup>10</sup> Laboratoire Détection, Capteurs et Mesures, Unité RDT, Ifremer Centre Bretagne - ZI de la Pointe du Diable - CS 10070 - 29280 Plouzané, France.

\* These authors contributed equally to this work.

32 **Abstract**

33 This paper presents two metazoan zooplankton datasets obtained by imaging samples collected on the Bay of  
34 Biscay continental shelf in spring during the PELGAS integrated surveys, over the 2004-2019 period. The samples  
35 were collected at night, with a WP2 200  $\mu\text{m}$  mesh size fitted with a Hydrobios (back-run stop) mechanical  
36 flowmeter, hauled vertically from the sea floor to the surface with a maximum depth set at 100 m when the  
37 bathymetry is deeper. The first dataset originates from samples collected from 2004 to 2016, imaged on land with  
38 the ZooScan and is composed of 1,153,507 imaged and measured objects. The second dataset originates from  
39 samples collected from 2016 to 2019, imaged on board the R/V *Thalassa* with the ZooCAM and is composed of  
40 702,111 imaged and measured objects. The imaged objects are composed of zooplankton individuals, zooplankton  
41 pieces, non-living particles and imaging artefacts, ranging from 300  $\mu\text{m}$  to 3.39 mm Equivalent Spherical  
42 Diameter, individually imaged, measured and identified. Each imaged object is geolocated, associated to a station,  
43 a survey, a year and other metadata. Each object is described by a set of morphological and grey level based  
44 features (8 bits encoding, 0 = black, 255 = white), including size, automatically extracted on each individual image.  
45 Each object was taxonomically identified using the web based application Ecotaxa with built-in, random forest  
46 and CNN based, semi-automatic sorting tools followed by expert validation or correction. The objects were sorted  
47 in 172 taxonomic and morphological groups. Each dataset features a table combining metadata and data, at the  
48 individual object granularity, from which one can easily derive quantitative population and communities  
49 descriptors such as abundances, mean sizes, biovolumes, biomasses, and size structure. Each object's individual  
50 image is provided along with the data. These two datasets can be used combined together for ecological studies as  
51 the two instruments are interoperable, or as training sets for ZooScan and ZooCAM users. The data presented here  
52 are available in the SEANOE dataportal: <https://doi.org/10.17882/94052> (ZooScan dataset, Grandremy et al.,  
53 2023c) and <https://doi.org/10.17882/94040> (ZooCAM dataset, Grandremy et al., 2023d).

54 **Keywords**

55 Zooplankton, ZooCAM, ZooScan, Bay of Biscay, imaging, PELGAS surveys.

56

## 57 **1 Introduction**

58 Metazoan planktonic organisms, hereafter referred to as zooplankton, encompass an immense diversity  
59 of life forms, which have successfully colonized the entire ocean, from eutrophic estuarine shallow areas to  
60 oligotrophic open ocean, from sunlit ocean to hadal depth. Their body sizes span five to six orders of magnitude  
61 in length, from  $\mu\text{m}$  to tens of meters (Sieburth & Smetacek, 1978). Zooplankton plays a pivotal role in marine  
62 ecosystem (Banse, 1995). It transfers the organic matter produced in the epipelagic domain by photosynthesis to  
63 the deeper layers of the ocean (Siegel et al., 2016), by producing fast sinking aggregates (Turner, 2015), and by  
64 diel vertical migration (Steinberg et al., 2000; Ohman & Romagnan, 2016). Zooplankton therefore participates in  
65 mitigating the anthropogenic carbon dioxide build up in the atmosphere responsible for climate change. Moreover,  
66 zooplankton is an exclusive trophic resource for commercially important fish during their larval stage, where a  
67 shift in zooplankton species or phenology can have dramatic effects on recruitment (i.e. North Sea cod, Beaugrand  
68 et al., 2003). In addition, it is a major trophic resource for adult planktivorous small pelagic fish, known as forage  
69 fishes (Van der Lingen, 2006). Recent studies suggest that zooplankton dynamics may have a significant effect on  
70 small pelagic fish population dynamics and individual body condition (Brosset et al., 2016; Menu et al., 2023),  
71 and therefore impact wasp-waist ecosystem based fisheries and fisheries dependent socio-ecosystems, worldwide  
72 (Cury et al., 2000).

73 Despite zooplankton being of such global importance in both climate change effects on ecosystems and  
74 management of fisheries (Chiba et al., 2018; Lombard et al., 2019), it is still technically difficult to monitor, with  
75 respect to other marine ecological compartments. Zooplankton biomass, diversity and spatio-temporal  
76 distributions cannot be estimated from spaceborne sensors as phytoplankton's does (Uitz et al., 2010), and  
77 zooplankton commercial exploitation data do not exist yet, as fish data does. One noticeable exception is the CPR  
78 surveys network that enables zooplankton data generation at spatio-temporal scales resolved enough to study  
79 climate change and diversity related zooplanktonic processes (Batten et al., 2019). Yet, generating zooplankton  
80 data often requires dedicated surveys at sea, specific sampling instruments and trained taxonomic analysts.  
81 Moreover, besides actual observation, modelling zooplankton remains a challenging task due to the diversity of  
82 traits such as life forms, life cycles, body sizes and physiological processes exhibited by zooplankton (Mitra &  
83 Davis 2010; Mitra et al., 2014). However, over the past two decades the development of imaging and associated  
84 machine learning semi-automatic identification tools (Irisson et al., 2022) have greatly improved the capability of  
85 scientists to analyse long (Feuilloley et al., 2022), high frequency (Romagnan et al., 2016), or spatially resolved  
86 (Grandremy et al., 2023a) zooplankton time series, as well as trait based data (Orenstein et al., 2022). Imaging and  
87 machine learning have particularly enabled the increased development of combined size and taxonomy  
88 zooplankton ecological studies (i.e. Vandromme et al., 2014; Romagnan et al., 2016; Benedetti et al., 2019). Yet,  
89 use of these machine learning tools is not trivial because these require abundant, scientifically qualified, sensor  
90 specific, training image data (i.e. learning set and test set, Irisson et al., 2022), and complex hardware and software  
91 setups (Panaiotis et al., 2022). One good example of such image dataset is the ZooScanNet dataset (Elineau et al.,  
92 2018), which features an extensive ZooScan (Gorsky et al., 2010) imaging dataset usable as a training set for  
93 ecologists as well as for imaging and machine learning scientists.

94 The objective of this paper is to present two freely available zooplankton imaging datasets, originating  
95 from two different instruments, the ZooScan (Gorsky et al., 2010), and the ZooCAM (Colas et al., 2018). These

96 datasets originate from the PELGAS integrated survey in the Bay of Biscay (Doray et al., 2018a), a continental  
97 shelf ecosystem supporting major European fisheries (ICES, 2021). Combined together, these datasets make up a  
98 16-years time series of sized and taxonomically resolved zooplankton, along with context metadata allowing the  
99 calculation of quantitative data, covering the whole Bay of Biscay continental shelf, from the French coast to the  
100 continental slope, and from the Basque country to southern Brittany, in spring. These datasets can be used for  
101 ecological studies (Grandremy et al., 2023a), machine learning studies, and modelling studies.

## 102 **2 Methods**

### 103 **2.1 Sampling**

104 Zooplankton samples were collected during the successive PELGAS (PELagique GAScogne) integrated  
105 surveys carried out over the Bay of Biscay (BoB) French continental shelf, every year in spring from 2004 to 2019  
106 on board the R/V *Thalassa*. The aim of this survey is to assess small pelagic fish biomass and monitor the pelagic  
107 ecosystem to inform ecosystem based fisheries management. Fish data, hydrology, phyto- and zoo-plankton  
108 samples and megafauna sightings (marine mammals and seabirds) are concomitantly collected to build long-term  
109 spatially resolved time series of the BoB pelagic ecosystem. The PELGAS sampling protocols combine day-time  
110 en-route data collection (small pelagic fish and megafauna), with night-time, depth integrated hydrology and  
111 plankton sampling at fixed points. Detailed PELGAS survey protocols can be found in Doray et al. (2018a) and  
112 Doray et al. (2021). The PELGAS survey datasets providing hydrological, primary producers, fish and megafauna  
113 data are available as gridded data in the SEANOE dataportal (Doray et al., 2018b) under the following link:  
114 <https://www.seanoe.org/data/00422/53389/>.

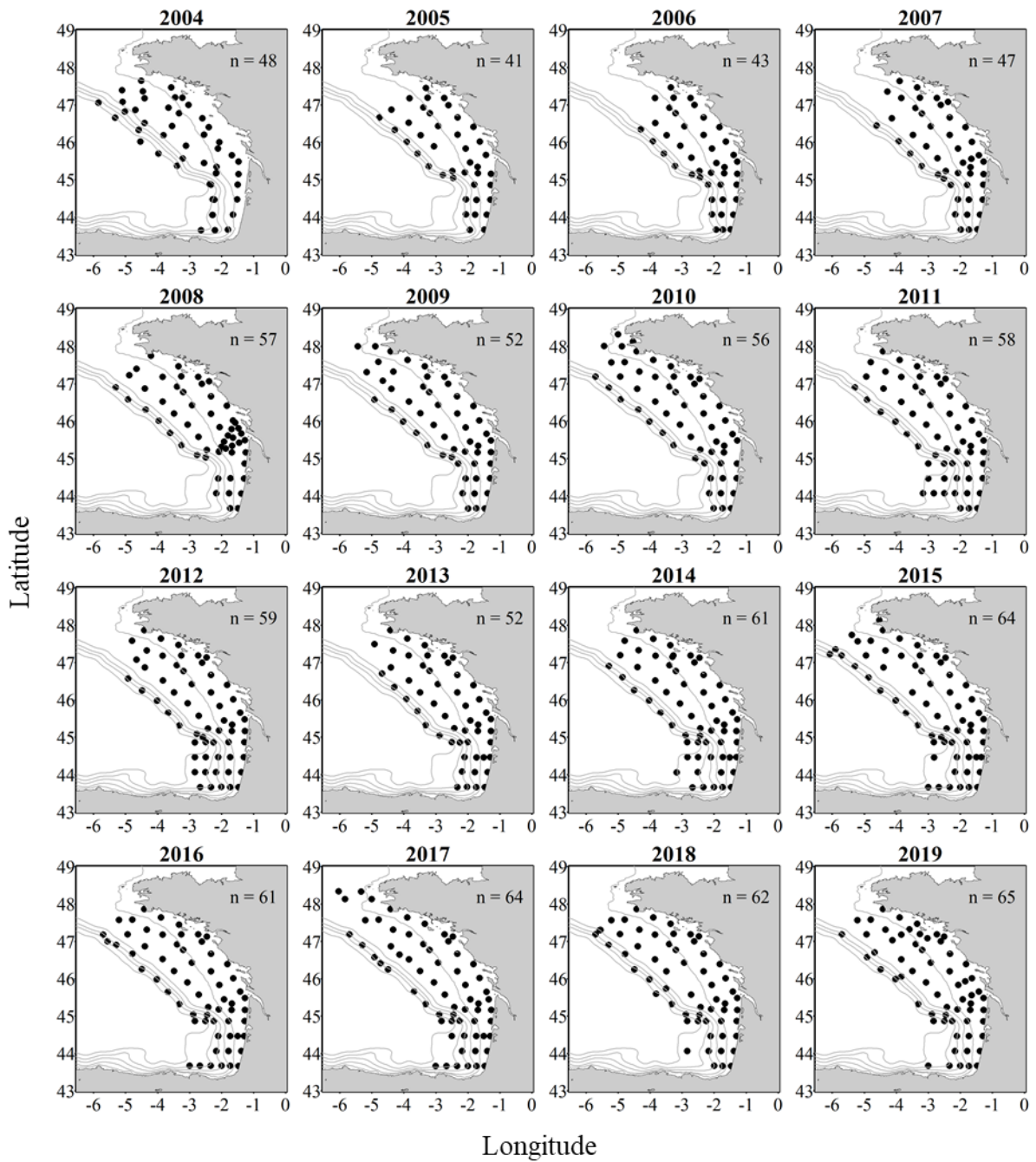
115 The number of zooplankton samples across years varied between 41 (2005) and 64 (2019), due to  
116 adjustments in the sampling strategy and weather conditions, for 889 zooplankton samples collected in total. From  
117 2004 to 2006, samples were collected in the southern Bay of Biscay until the Loire estuary only (Fig. 1). Sampling  
118 was carried out in vertical tows during night time using a 200- $\mu$ m mesh size WP2 net, generally from 100 m depth  
119 (or 5 m above the seabed) to the surface. In 2004 and 2005, the targeted maximum sampling depth was 200 m. In  
120 2004, fifteen samples were collected deeper than 100 m, among which eleven were deeper than 120 m; in 2005,  
121 twenty samples were collected deeper than 100 m, among which thirteen were deeper than 120 m. Before 2014,  
122 the sampled water volume was estimated by multiplying the cable length by the net opening surface (0.25 m<sup>2</sup>)  
123 whereas since 2014, the net was equipped with a Hydrobios back-run stop flowmeter. The samples originating  
124 from 2004 to 2016 surveys were preserved in 4% formaldehyde (final concentration) and analysed on land in the  
125 laboratory with the ZooScan, while since 2016 they were analysed live on board with the ZooCAM.

### 126 **2.2 Sample processing and analyses**

#### 127 **2.2.1 Digitization with the ZooScan**

128 Preserved samples were digitized with the ZooScan (Gorsky et al., 2010), a flatbed scanner generating  
129 16-bit gray-level high-resolution images (2400 dpi, pixel size: 10.56  $\mu$ m, image size: 15 $\times$ 24 cm equivalent to  
130 14 200 $\times$ 22 700 pixels). It is well suited for the imaging of preserved organisms ranging in size from 300  $\mu$ m to  
131 several centimeters. The ZooScan is run by the custom made, ImageJ based, ZooProcess software which generates  
132 one single large image for each scan that contains up to 2000 organisms depending on the size of the imaged  
133 organisms.

134           Prior to digitization, the seawater and formaldehyde solution was filtered through a 180  $\mu\text{m}$  mesh sieve  
135 into a trash tank, under a fume hood. The organisms were then gently but thoroughly rinsed with freshwater over  
136 the tank, in the sieve. They were then size-fractionated with a 1 mm sieve, into organisms larger and smaller than  
137 1 mm size fractions. This size splitting step is recommended when using the ZooScan to address the possible  
138 under-representation of large objects bias caused by the necessary subsampling. Each size fraction was subsampled  
139 separately with a Motoda splitter to obtain two subsamples containing 500-1000 objects for the large organisms  
140 size fraction, and 1000-2000 objects for the small organisms size fraction. Each subsample was imaged after  
141 manual separation of objects on the scanning tray, to mitigate the number of overlapping objects as recommended  
142 in Vandromme et al. (2012). Overall, 699 samples were digitized following this protocol, corresponding to 1397  
143 scans (one sample was not size fractionated as it did not contained organisms larger than 1 mm).



144

145 Figure 1: Metazoan zooplankton sampling locations during the PELGAS cruises in the Bay of Biscay from 2004  
 146 to 2019. The years with the poorest coverage are 2005 and 2006 with 41 and 43 sampling stations respectively;  
 147 and the years with the best coverage are 2015, 2017 and 2019 with 64, 64 and 65 sampling stations respectively.

## 148 **2.2.2 Digitization with the ZooCAM**

149 The ZooCAM is an in-flow imaging instrument, designed to digitize preserved as well as live zooplankton  
150 samples, on board, immediately after net collection (Colas et al., 2018). The ZooCAM features a cylindrical  
151 transparent tank in which the zooplankton sample is mixed with filtered seawater. Depending on the richness of  
152 the sample, and the subsampling (if necessary), the volume of seawater can be adjusted between 2-7 litres. The  
153 organisms were pumped at a  $1\text{L}\cdot\text{min}^{-1}$  from the tank to a flowcell inserted between a CCD camera (pixel size:  $10.3$   
154  $\mu\text{m}$ ) and a red LED flashing device where they were imaged at 16 fps. Given the flowcell volume, the size of the  
155 field of view, the imaging frequency and the flowrate, all the seawater volume containing the organisms was  
156 imaged (Colas et al., 2018). Before all the initial volume was imaged, the tank and the tubing were carefully and  
157 thoroughly rinsed with filtered seawater to ensure the imaging of all the organisms poured in the tank. For each  
158 sample, the ZooCAM generates a stack of small size ( $\sim 1$  Mo) raw images that are subsequently analysed with the  
159 ZooCAM software. Depending on the initial water content of the tank and the rinsing, a ZooCAM run can generate  
160 up to 10k raw images from which the individual organism vignettes will be extracted. A ZooCAM run on a live  
161 sample often generates up to 5000-10000 vignettes of individual organisms. It is very important to subsample the  
162 initial samples with a dichotomic splitter (here a Motoda splitter), to get subsamples with a quantity of objects that  
163 reduce the risk of imaging overlapping objects, and avoid any dependency to the water volume imaged to  
164 reconstruct quantitative estimates of zooplankton as the initial and rinsing volume are variable. Overall, 190  
165 samples were digitized live on-board with the ZooCAM.

## 166 **2.3 Images processing**

167 Both instruments generate grey level working images (8 bit encoding, 0 = black, 255 = white). In both  
168 cases, image processing consisted in (i) a “physical” background homogenization by subtracting an empty  
169 background image to each sample image (1 for ZooScan, and as many as raw images for ZooCAM), (ii) a  
170 thresholding of each raw image (threshold value: 243 for ZooScan, 240 for ZooCAM), (iii) the segmentation of  
171 each object imaged. The ZooProcess software was set to detect and segment objects with an area equal or larger  
172 than 631 pixels, whereas the ZooCAM software was set to detect objects with an area equal or larger than 667  
173 pixels, which in both cases equals  $300\ \mu\text{m}$  ESD, or a biovolume of  $0.014\ \text{mm}^3$  (using a spherical biovolume model,  
174 Vandromme et al., 2012).

175 Morphological features were then extracted on each detected object. Features generated by the ZooScan  
176 are defined in Gorsky et al. (2010) and those generated by the ZooCAM are defined in Colas et al. (2018). ZooScan  
177 images were processed with ZooProcess v7.39 (04/10/2020) open source software. ZooCAM images were  
178 processed with the proprietary ZooCAM custom made software which uses the MIL (Matrox Imaging Library,  
179 Dorval, Québec, Canada) as the individual object processing kernel. Each detected object was finally cropped from  
180 the working sample images, and saved as a unique, labelled vignette, in a sample specific folder along with a  
181 sample specific single text file containing the objects features arranged as a table with objects arranged in lines  
182 and features in columns.

## 183 **2.4 Touching objects**

184 The ZooProcess features a tool that enable the digital separation of possible touching objects in the final  
185 image dataset, for each sample. As touching objects may impair the estimations of abundances and size structure

186 (Vandromme et al., 2012), remaining touching objects were searched for on the individual vignettes from the  
187 ZooScan and digitally manually separated with the ZooProcess separation tool to improve the quality of further  
188 identifications, counts and size structure of zooplankton. The ZooCAM software does not offer such a tool.

## 189 **2.5 Taxonomic identification of individual images**

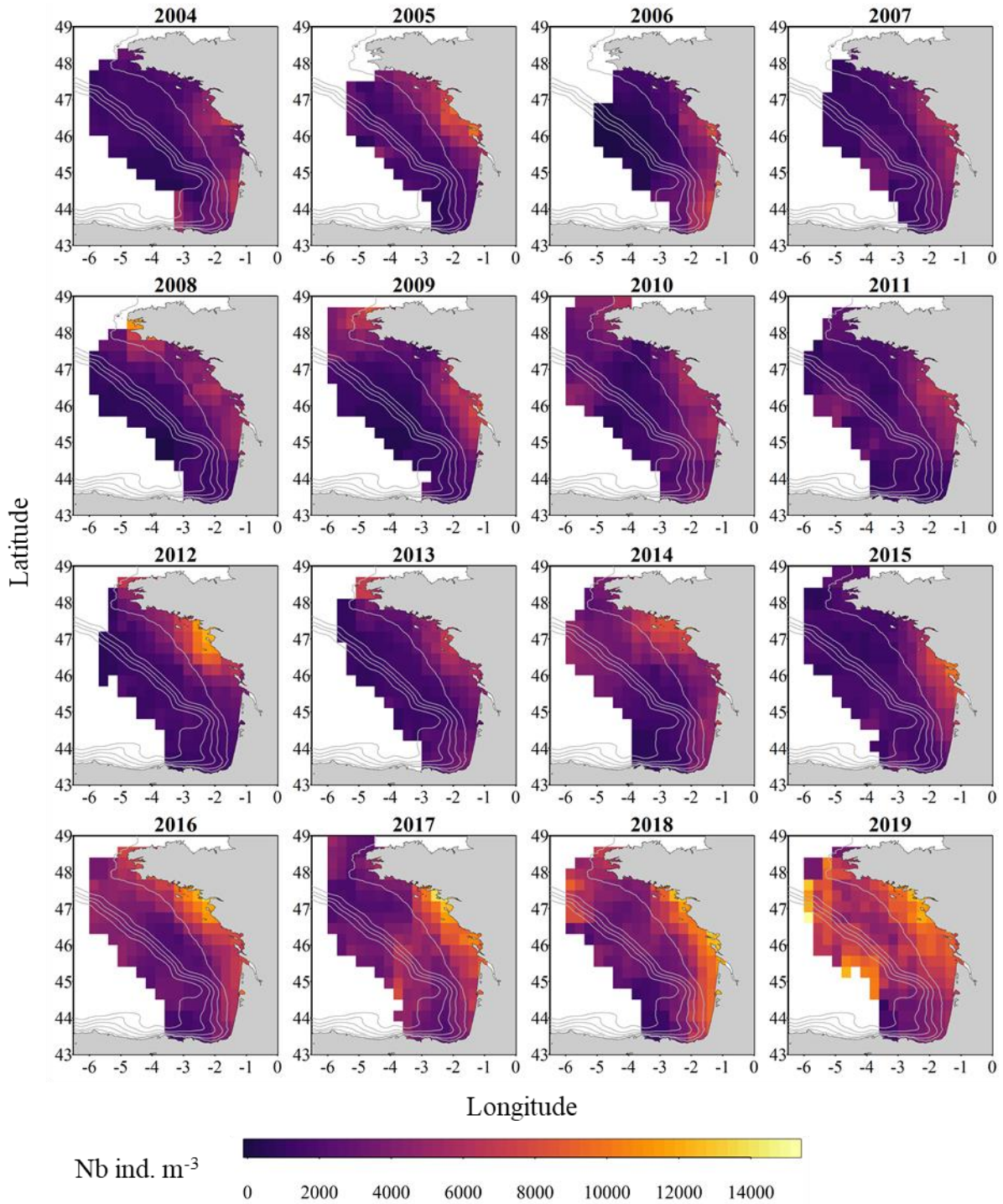
190 All individual vignettes from both instruments were sorted and identified with the help of the online  
191 application Ecotaxa (Picheral et al., 2017), as two instrument-specific separated sets. Ecotaxa features a Random  
192 Forest algorithm (Breiman, 2001) and a series of instruments specific tuned spatially sparse Convolutional Neural  
193 Networks (Graham, 2014) that were used in a combined approach to predict identifications of unidentified objects.  
194 First, an automatic classification of non-identified individual vignettes into coarse zooplankton and non-  
195 zooplankton categories was carried out. In both cases (ZooScan and ZooCAM), Ecotaxa hosted instrument specific  
196 image datasets, previously curated and freely available, that were used as initial learning sets. These initial  
197 classifications were then visually inspected, manually validated or corrected when necessary, and taxonomically  
198 refined when possible. After a few thousand images were validated in each project, they were used as dataset  
199 specific learning sets to improve the initial coarse automatic identifications. This process was iterated until all the  
200 individual vignettes were classified into their maximum reachable taxonomical detail. A subsequent quality check  
201 of automatic taxonomic identifications has been realized in a two-step process: a first complete review (validation  
202 and / or correction) of all individual automatic identifications was done by GN and RJB; then, trained experts (JL  
203 and NA) reviewed and curated the ZooScan and the ZooCAM datasets, respectively, at the individual level.  
204 Although some identification errors may still remain in the datasets, we consider this double check process as  
205 sufficient to provide taxonomically qualified data.

## 206 **2.6 Intercalibration of the two instruments**

207 The two datasets are usable separately. However, considered together they build a 16 years long spatio-  
208 temporal time series. A comparison study was done to ensure these datasets are homogeneous and can thus be  
209 combined for ecological studies (Grandremy et al., 2023b). All the zooplankton samples from year 2016 (61  
210 sampling stations over the whole BoB continental shelf) were imaged with both instruments. In brief, all non-  
211 zooplankton and touching objects images were removed from the initial datasets. Then, the interoperable size  
212 range was determined with an assessment based on the comparison of Normalized Biovolume – Size Spectra (NB-  
213 SS) for each instrument. This size interval ranges between [0.3-3.39] mm ESD. Finally, the zooplankton  
214 communities as seen by the ZooScan and the ZooCAM were compared by taxa and by station using 27 taxonomic  
215 groups. Poorly represented taxa as well as non-taxonomically identified objects were not taken into account in the  
216 zooplankton variables computation and in community structure analyses. Both instruments showed similar NB-  
217 SS slopes for 58 out of 61 stations; depicted equivalent abundances, biovolumes and mean organisms' sizes, as  
218 well as similar community composition for a majority of sampling stations. They also estimated similar spatial  
219 patterns of the zooplankton community at the scale of the Bay of Biscay. However, some taxonomic groups showed  
220 discrepancies between instruments, which originates from the differences in sample preparation protocols before  
221 the image acquisition, the imaging techniques and quality, and whether the samples were imaged live or fixed. For  
222 example, the mineralized protists (here, Rhizaria) dissolve in formalin and are considered underestimated in  
223 preserved seawater samples (Biard et al., 2016). Also, the random orientation of objects in the ZooCAM flow cell  
224 leads to a loss of taxonomic identification accuracy due to the difficulty to spot the specific features needed for the

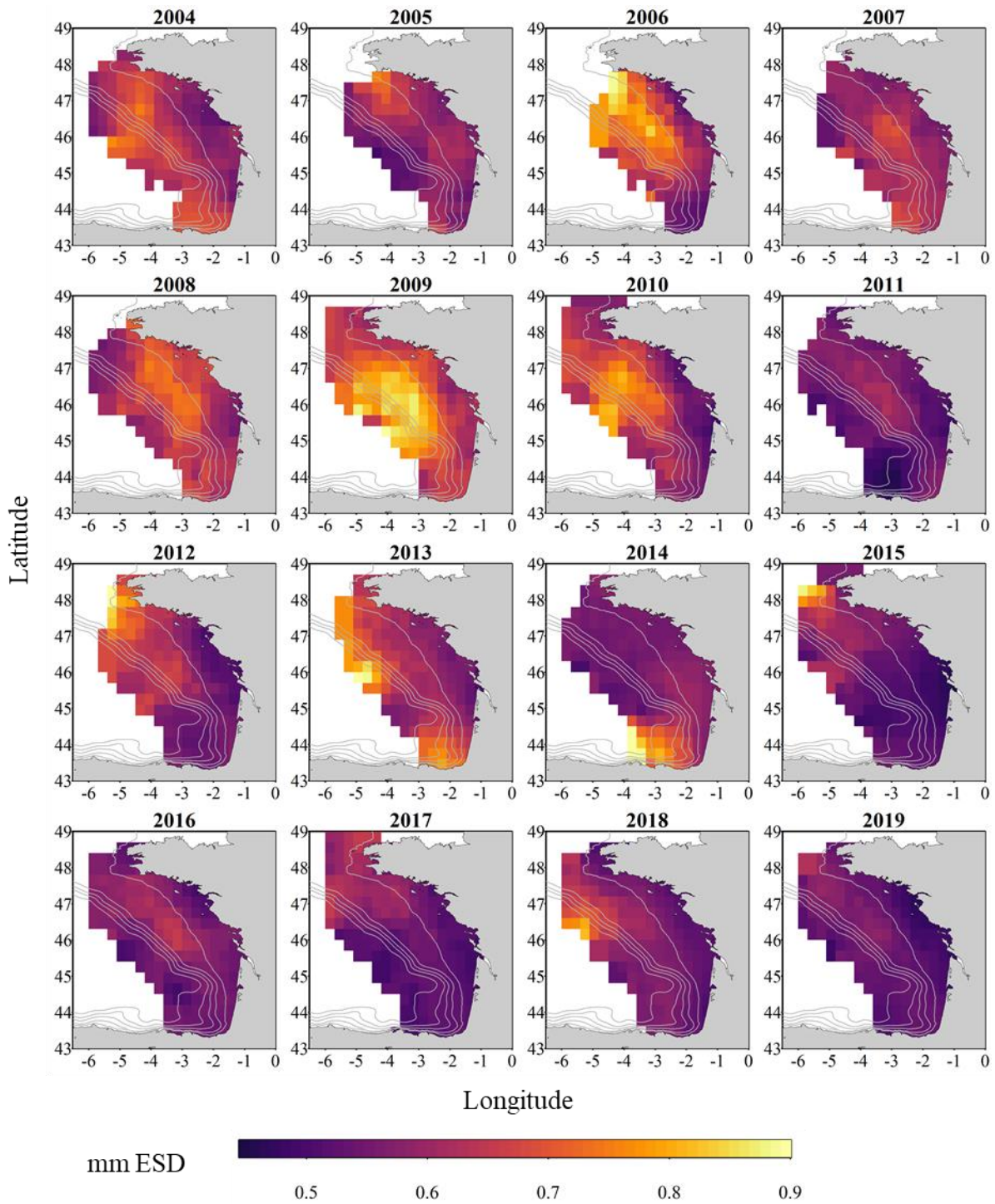


225 identification (Colas et al., 2018; Grandremy et al., 2023b). This is particularly acute for copepods, where the  
226 ZooScan seems to provide better identification capabilities to experts, as the organisms are imaged in a lateral  
227 view most of the time whereas the ZooCAM often images them in a non-lateral, randomly-oriented view,  
228 preventing the visualisation of specific features. A detailed discussion about how to explain the discrepancies  
229 between the ZooScan and the ZooCAM can be found in Grandremy et al. (2023b). We assume that the two  
230 presented datasets build a single, 16 years long spatio-temporal time series of abundances (Fig. 2) and sizes of  
231 zooplanktonic organisms (Fig. 3), from which biovolumes, biomasses, Shannon index (Fig. 4), and zooplankton  
232 community size structure can be derived (Vandromme et al., 2012).



233

234 Figure 2: Gridded maps of total zooplankton abundances expressed as individuals per cubic meters of sampled  
 235 seawater, during the PELGAS cruises in the Bay of Biscay from 2004 to 2019. The abundances are well within  
 236 the range of zooplankton abundances seen over other temperate continental shelves. They exhibit a marked coastal  
 237 to offshore gradient, abundances being higher at the coast. Abundances also show an overall increase over the  
 238 years. The gridding procedure is presented in Petitgas et al. (2009) and Petitgas et al. (2014). See also Doray et al.  
 239 (2018c) and Grandremy et al. (2023a) for application examples.



240

241 Figure 3: Gridded maps of total zooplankton mean sizes expressed as mm Equivalent Spherical Diameter during  
 242 the PELGAS cruise in the Bay of Biscay from 2004 to 2019. They exhibit a coastal to offshore gradient as well as  
 243 a north-south gradient. Mean body sizes are smaller at the coast and usually smaller in the south. In general, mean  
 244 body sizes show an overall decrease over the years. The gridding procedure is presented in Petitgas et al. (2009)  
 245 and Petitgas et al. (2014). See also Doray et al. (2018c) and Grandremy et al. (2023a) for application examples.

## 246 **3 Datasets**

### 247 **3.1 Taxonomic groups and Operational Morphological Groups**

248 The ZooScan dataset is composed of 1,153,507 zooplankton individuals, zooplankton parts, non-living  
249 particles and imaging artefacts individually imaged and measured with the ZooScan and ZooProcess (Gorsky et  
250 al., 2010), sorted in 127 taxonomic and morphological groups. The ZooCAM dataset is composed of 702,111  
251 zooplankton individuals, zooplankton parts, non-living particles and imaging artefacts individually imaged and  
252 measured with the ZooCAM (Colas et al., 2018), sorted in 127 taxonomic and morphological or life stages groups.  
253 The total number of different groups identified with both instruments combined is 170, among which 84 are in  
254 common (Table 1), 43 belong to the ZooScan dataset only and 43 others belong to the ZooCAM dataset only  
255 (Table 2). The identified groups were divided into actual taxa and Operational Morphological Groups (OMGs).  
256 Typically, OMGs are either non-adult life stages of taxa, aggregated morphological groups, or non-living groups  
257 (see Tables 1 and 2). Among the groups common to both instruments, 45 are actual taxa, and 39 are OMGs (Table  
258 1). Among the ZooScan only groups, 22 are taxa, and 21 are OMGs, and among the ZooCAM only groups, 18 are  
259 taxa, and 25 are OMGs (Table 2).

260 The differences in identified groups, in the ratio taxa/OMGs, and in the associated counts arose from  
261 several aspects of the data generation. Firstly, the two imaging methods differ in their technical set-up. The main  
262 difference is that, on the one hand, fixed organisms are laid down and arranged manually on the imaging sensor  
263 and digitized in a lab, steady 2-D, set-up when using the ZooScan. On the other hand, organisms are imaged live,  
264 in a moving fluid, in a 3-D environment (the flowcell), on-board when digitized with the ZooCAM. Their position  
265 in front of the camera may not enable an identification as precise as when they are laid on the scanner tray  
266 (Grandremy et al., 2023b; Colas et al., 2018). Secondly, the dataset are sequential in time, the ZooCAM dataset  
267 follows the ZooScan's. Zooplankton communities in the Bay of Biscay may have changed over time, even if their  
268 biomass as aggregated groups show a remarkable space-time stability (Grandremy et al., 2023a). Thirdly, we  
269 cannot guaranty that there is no adverse effect on taxonomic identification, as validation involved several experts  
270 (Culverhouse, 2007). Although we paid great attention to homogenize the final detailed datasets, we recommend  
271 to aggregate taxa and OMGs and reduce the biological resolution for ecological studies (Grandremy et al., 2023a,  
272 2023b). Additionally, numerous identified and sorted taxa and OMGs do not belong to the metazoan zooplankton,  
273 or are non-adult life stages, or parts of organisms. Those were included in the presented datasets because they are  
274 always found in natural samples. They need to be separated from entire organisms to ensure as accurate as possible  
275 abundances estimations, as well as taken into account to ensure accurate biovolumes or biomasses estimations. A  
276 good example is the siphonophore issue: numerous swimming bells of degraded siphonophores individuals can be  
277 found and imaged in a sample. Determining an accurate siphonophore abundance may not be easy, but this could  
278 be overcome by considering the biovolume or biomass of siphonophores by adding up the numerous parts'  
279 biovolumes or biomass of the organisms imaged.

280 Table 1: ZooCAM and ZooScan common taxa and Operational Morphological Groups (OMGs). Taxa are listed  
 281 in the left column of the table, and OMGs are listed in the right column of the table . OMGs names are spelled as  
 282 they appear in the dataset. Numbers next to each taxa and OMGs are the counts and the percentages (%) for each  
 283 category for each instrument in the whole datasets. Non-zooplanktonic OMGs are highlighted in bold, and genera  
 284 and species are formatted in italics.

taxa	ZooCAM		ZooScan		OMG	ZooCAM		ZooScan	
	counts	%	counts	%		counts	%	counts	%
Calanoida	137536	19.588	149956	13.00	<b>detritus</b>	105751	15.06	219541	19.03
Oithonidae	112977	16.09	110510	9.58	<i>diatoma</i>	36842	5.25	1084	0.09
Acartiidae	30403	4.33	66353	5.75	<b>bubble</b>	32563	4.64	1112	0.10
Temoridae	13520	1.93	31335	2.72	<b>Noctiluca_Noctiluaceae</b>	22165	3.16	20784	1.80
Oncaeidae	11843	1.69	34651	3.00	other_living	15029	2.14	5861	0.51
Calanidae	9578	1.36	91513	7.93	dead_copepoda	13383	1.91	17151	1.49
Limacinidae	8966	1.28	6423	0.56	<b>fiber_detritus</b>	13379	1.91	25124	2.18
Appendicularia	6724	0.96	34027	2.95	nauplii_cirripedia	6766	0.96	6008	0.52
Cladocera	5590	0.80	18213	1.58	gonophore_diphyidae	4395	0.63	1462	0.13
Centropagidae	4592	0.65	14651	1.27	multiple_copepoda	3740	0.53	961	0.08
<i>Neoceratium</i>	2984	0.43	4830	0.42	nauplii_crustacea	3422	0.49	10747	0.93
Euchaetidae	2643	0.38	12957	1.12	<b>artefact</b>	2643	0.38	60718	5.26
Metridinidae	2333	0.33	15081	1.31	multiple_other	1928	0.27	10303	0.89
Corycaeidae	2021	0.29	4720	0.41	pluteus_echinodermata	1623	0.23	1441	0.12
<i>Euterpina</i>	1043	0.15	2870	0.25	calyptopsis_euphausiacea	1396	0.20	3246	0.28
Euphausiacea	889	0.13	1195	0.10	bivalvia_mollusca	1324	0.19	3766	0.33
<i>Calocalanus</i>	820	0.12	1196	0.10	bract_diphyidae	1315	0.19	386	0.03
Chaetognatha	624	0.09	7274	0.63	cypris	862	0.12	2363	0.20
Harpacticoida	481	0.07	1697	0.15	nectophore_diphyidae	839	0.12	14389	1.25
<i>Obelia</i>	459	0.07	1016	0.09	<b>egg_actinopterygii</b>	768	0.11	3596	0.31
Annelida	256	0.04	2434	0.21	tail_appendicularia	753	0.11	11349	0.98
Decapoda	173	0.02	471	0.04	cyphonaute	684	0.10	2218	0.19
<i>Microsetella</i>	116	0.02	1169	0.10	eudoxie_diphyidae	501	0.07	69	0.01
Phoronida	90	0.01	163	0.01	larvae_echinodermata	483	0.07	2200	0.19
Actinopterygii	85	0.01	2113	0.18	part_siphonophorae	279	0.04	12976	1.12
Candaciidae	70	0.01	2773	0.24	larvae_annelida	244	0.03	708	0.06
Amphipoda	68	0.01	853	0.07	<b>egg_sac_egg</b>	152	0.02	394	0.03
Tomopteridae	58	0.01	618	0.05	zoeta_decapoda	151	0.02	1405	0.12
Ostracoda	55	0.01	341	0.03	cnidaria_metazoa	148	0.02	4974	0.43
Doliolida	26	< 0.01	128	0.01	larvae_porcellanidae	127	0.02	2838	0.25
Echinodermata	24	< 0.01	253	0.02	nectophore_physonectae	106	0.02	696	0.06
Aetideidae	15	< 0.01	75	0.01	ctenophora_metazoa	94	0.01	126	0.01
<i>Branchiostoma</i>	15	< 0.01	210	0.02	<b>egg_unkn temp_Engrauidae temp</b>	61	0.01	192	0.02
Thecosomata	15	< 0.01	59	0.01	part_ctenophora	30	< 0.01	319	0.03
Heterorhabdidae	8	< 0.01	205	0.02	tornaria larvae	21	< 0.01	83	0.01
Pontellidae	6	< 0.01	299	0.03	<b>egg_other</b>	17	< 0.01	2281	0.20
Cumacea	4	< 0.01	180	0.02	megalopa	6	< 0.01	460	0.04
Mysida	3	< 0.01	885	0.08	<b>scale</b>	2	< 0.01	53	< 0.01
Eucalanidae	2	< 0.01	839	0.07	siphonula	1	< 0.01	20	< 0.01
Insecta	2	< 0.01	3	< 0.01					
Foraminifera	1	< 0.01	384	0.03					
<i>Haloptilus</i>	1	< 0.01	5	< 0.01					
Isopoda	1	< 0.01	123	0.01					
Rhincalanidae	1	< 0.01	127	0.01					
Sapphirinidae	1	< 0.01	21	< 0.01					

285

286

287 Table 2: ZooCAM and ZooScan not common taxa and Operational Morphological Groups (OMGs). Taxa and  
 288 OMGs appearing exclusively in the ZooCAM dataset are listed in the left column, those appearing exclusively in  
 289 the ZooScan dataset are listed in the right column. OMGs names are spelled as they appear in the dataset. Numbers  
 290 next to each taxa and OMG are the counts and the percentages (%) for each category for each instrument in the  
 291 whole datasets. Non-zooplanktonic taxa and OMGs are highlighted in bold, and genera and species are formatted  
 292 in italics.

ZooCAM			ZooScan		
taxa/OMG	counts	%	taxa/OMG	counts	%
<b>light_detritus</b>	38126	5.43	<b>badfocus_artefact</b>	34507	2.99
Rhizaria	13347	1.90	badfocus_Copepoda	11656	1.01
Copepoda X	6727	0.96	Eumalacostraca	9815	0.85
<b>fluffy_detritus</b>	3589	0.51	part_Crustacea	7530	0.65
<i>Evadne</i>	1889	0.27	Fritillariidae	3635	0.32
Hydrozoa	1674	0.24	trunk_appendicularia	1210	0.10
Poecilostomatoidea	1094	0.16	<i>Aglaura</i>	1113	0.10
Rhizaria X	857	0.12	<i>Pleuromamma</i>	695	0.06
<b>Rhizosolenids</b>	761	0.11	part_Cnidaria	692	0.06
dead_harpacticoida	528	0.08	zoaea_galatheidae	660	0.06
gelatinous	348	0.05	pluteus_ophiuroida	640	0.06
<b>Trichodesmium</b>	265	0.04	Salpida	470	0.04
<b>aggregata</b>	253	0.04	Harosa	374	0.03
<b>feces</b>	227	0.03	tail_chaetognatha	251	0.02
<b>Halosphaera</b>	193	0.03	<i>Euchirella</i>	239	0.02
<i>Podon</i>	162	0.02	protozoa_mysida	229	0.02
Diphyidae	144	0.02	<i>Solmundella bitentaculata</i>	178	0.02
larvae_gastropoda	116	0.02	Peltidiidae	133	0.01
<b>chainlarge</b>	114	0.02	<i>Liriope tetrphylla</i>	121	0.01
veliger	113	0.02	part_Annelida	121	0.01
egg 1 temp_Sardina temp	100	0.01	larvae_crustacea	114	0.01
egg 1 temp_Engraulidae temp	65	0.01	larvae_mysida	73	0.01
Isias	51	0.01	ephyra_scyphozoa	64	0.01
egg 2 3 temp_Sardina temp	49	0.01	actinula_hydrozoa	49	< 0.01
Calycophorae	30	< 0.01	part_thaliacea	44	< 0.01
egg 9 11 temp_Sardina temp	26	< 0.01	<i>Atlanta</i>	43	< 0.01
egg unkn temp_Sardina temp	23	< 0.01	like_laomedidae	36	< 0.01
<i>Calocalanus tenuis</i>	17	< 0.01	Nemertea	31	< 0.01
egg 4 6 temp_Sardina temp	15	< 0.01	protozoa_penaeidae	28	< 0.01
egg 9 11 temp_Engraulidae temp	14	< 0.01	Cavoliniidae	21	< 0.01
egg 7 8 temp_Engraulidae temp	13	< 0.01	Actinaria	13	< 0.01
Enteropneusta_Hemichordata	12	< 0.01	pilidium_nemertea	12	< 0.01
<b>Chaetoceros sp.</b>	9	< 0.01	protozoa_sergestidae	12	< 0.01
head_crustacea	9	< 0.01	phyllosoma	8	< 0.01
<i>Centropages hamatus</i>	8	< 0.01	Creseidae	7	< 0.01
Thaliacea	7	< 0.01	Penaeoidea	7	< 0.01
egg 4 6 temp_Engraulidae temp	6	< 0.01	Paguridae	4	< 0.01
Sphaeronectidae	4	< 0.01	larvae_squillidae	4	< 0.01
<i>Thalassionema</i>	4	< 0.01	Cephalopoda	3	< 0.01
egg 2 3 temp_Engraulidae temp	3	< 0.01	<i>Cymbulia peroni</i>	3	< 0.01
<i>Jaxea</i>	2	< 0.01	Nannosquillidae	2	< 0.01
<i>Pyrosoma</i>	1	< 0.01	<i>Lubbockia</i>	1	< 0.01
larvae_ascidiacea	1	< 0.01	Monstrilloida	1	< 0.01

293

294

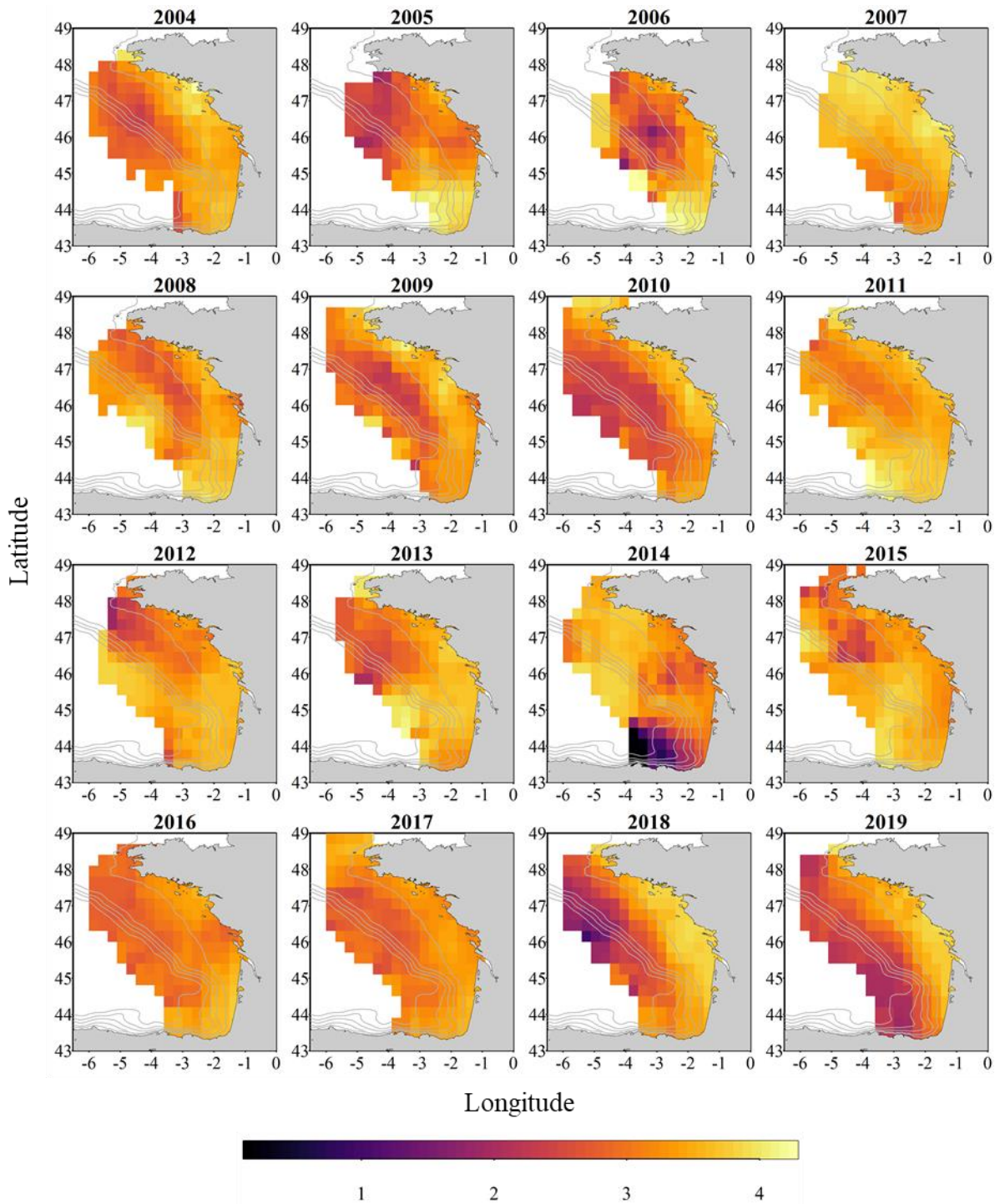
295 OMGs' names are mainly in the form of two words separated by a "<" character. Although we tried to name them  
 296 as most explicitly as possible, a few potentially needed clarifications can be found in Table 3.

297 Table 3: Non-exhaustive list of prefixes, their types (morphological, developmental stage, taxonomical, non-living  
 298 and imaging artefact), and content.

prefix	type	content of category
bract	morphological	single siphonophorae bracts
eudoxie	morphological	single siphonophorae eudoxia zooids
gonophore	morphological	single siphonophorae gonozooids
nectophore	morphological	single siphonophorae swimming bells
trunk	morphological	single appendicularian trunks detached from their tails
tail	morphological	appendicularian's or chaetognath's tail shaped part of the body
head	morphological	individual organisms' heads detached from the body
part	morphological	unidentified body part
egg sac	morphological	detached copepod egg sacs
like	morphological	look alike, without absolute certainty
multiple	morphological	two or more objects touching each other in the same vignette
other	morphological	non-identified living object
actinula	developmental stage	undefined hydrozoa actinula larval stage
calyptopsis	developmental stage	Euphausiacea calyptopsis larval stage
egg	developmental stage	egg larval stage
ephyra	developmental stage	ephyra hydrozoa larval stage
larvae	developmental stage	undefined larval stage
nauplii	developmental stage	crustacean nauplii larval stage
pilidium	developmental stage	free-swimming larvae of nemertean worm
protozoa	developmental stage	crustacean protozoa larval stage
pluteus	developmental stage	Echinodermata pluteus larval stage
zoa	developmental stage	crustacean zoea larval stage
egg 1 temp	developmental stage	clupeid fish embryo developmental stage 1*
egg 2 3 temp	developmental stage	clupeid fish embryo developmental stages 2 and 3 aggregated*
egg 4 6 temp	developmental stage	clupeid fish embryo developmental stages 4 to 6 aggregated*
egg 7 8 temp	developmental stage	clupeid fish embryo developmental stages 7 and 8 aggregated*
egg 9 11 temp	developmental stage	clupeid fish embryo developmental stages 9 to 11 aggregated*
egg unknown	developmental stage	clupeid fish unidentified embryo developmental stage*
Bivalvia	taxonomical	small bivalve larvae of unidentified mollusca
dead	non-living	copepod's exuvia, carcass or part of dead body
fiber	non-living	fiber like detritus
fluffy	non-living	very porous detritic particles
light	non-living	very transparent detritic particles
299 badfocus	imaging artefact	out-of-focus objects

300

301 \* clupeids fish embryo developmental stages according to Ahlstrom (1943) and Moser & Ahlstrom (1985).



302

303 Figure 4: Gridded maps of total zooplankton Shannon index (calculated on spherical biovolumes) during the  
 304 PELGAS cruise in the Bay of Biscay from 2004 to 2019. Shannon index exhibit a coastal to offshore gradient as  
 305 well as a north-south gradient. Shannon index is larger at the coast and in the south, except in 2014 where it is  
 306 smaller in the south, offshore. The gridding procedure is presented in Petitgas et al. (2009) and Petitgas et al.  
 307 (2014). See also Doray et al. (2018c) and Grandremy et al. (2023a) for application examples.



## 308 3.2 Data and images

### 309 3.2.1 Data

310 The data is divided into two datasets available as tab separated files, one for each instrument. Within each  
311 dataset the data is organized as a table containing text data as well as numerical data. Each dataset combines  
312 together actual data and metadata at the individual object granularity. For each object, the user will be able to find  
313 descriptors originating from the image processing (i.e. features), and sampling metadata (i.e. latitude and longitude  
314 of sampling station, date and time of sampling, sampling device, etc.) and sample processing metadata (i.e.  
315 subsampling factor, seawater sampled volume, pixel size), in columns, and individual objects in lines. The columns  
316 headers are defined in Tables A1 and A2 for ZooCAM and ZooScan datasets respectively. The following prefixes  
317 enable the segregation of types of data and metadata: (i) “object\_”, which identifies variables assigned to each  
318 object individually; (ii) “sample\_”, which identifies variables assigned to each sample; (iii) “acq\_”, which  
319 identifies variables assigned to each data acquisition for the same sample (note here that this type of variable is  
320 found only in the ZooScan dataset as ZooScan samples were splitted in two size fractions corresponding to two  
321 acquisitions); (iv) “process\_”, which identifies variables describing key image processing features (i.e. pixel size).  
322 Those prefixes originate from the use of the Ecotaxa web application to sort and identify the images (Picheral et  
323 al., 2017) that promote this specific formatting. The ZooCAM dataset is shaped as a 72 columns (variables) x  
324 702,111 rows (individual imaged objects) matrix and the ZooScan dataset is shaped as a 71 columns (variables) x  
325 1,153,507 rows (individual imaged objects) matrix.

326 Among the 70+ variables it is worth noticing the following ones:

- 327 (i) objid: it is a unique individual object numerical identifier that enables to link single data line to a  
328 corresponding single image in the image dataset;
- 329 (ii) taxon: it is the taxonomic or OMG identification of the imaged objects written as they appear in the  
330 Tables 1 and 2;
- 331 (iii) lineage: it is the full taxonomic lineage of the taxon. Lineage may be used to aggregate taxa at a higher  
332 taxonomic levels, respecting taxonomic lineages;
- 333 (iv) classif\_id: it is a unique, numerical, taxon identifier;
- 334 (v) sample\_sub\_part / acq\_sub\_part: those are the subsampling ratios, for ZooCAM and ZooScan  
335 respectively, needed to reconstruct the quantitative estimates of the samples’ abundances;
- 336 (vi) sample\_fishingvolume / sample\_tot\_vol: those are the total seawater sampled volumes for ZooCAM  
337 and ZooScan respectively, needed to normalize the samples’ concentrations by seawater volume.

338 One can therefore calculate quantitative abundances estimates for a taxon in a sample as follow:

$$339 \text{ ZooCAM: } Ab_{\text{taxon}} = \frac{n_{\text{taxon}} \times \text{sample\_sub\_part}}{\text{sample\_fishingvolume}} \quad (1)$$

$$340 \text{ ZooScan: } Ab_{\text{taxon}} = \frac{(n_{\text{taxon}_{\text{acq1}}} \times \text{acq\_sub\_part}_{\text{acq1}}) + (n_{\text{taxon}_{\text{acq2}}} \times \text{acq\_sub\_part}_{\text{acq2}})}{\text{sample\_tot\_vol}} \quad (2)$$

341 Where  $Ab$  is the abundance in  $\text{ind.m}^{-3}$  and  $n$  is the number of individuals for “taxon”.

### 342 **3.2.2 Images**

343 Two sets of individual images sorted into folders by categories (Tables 1 and 2) come along with each  
344 dataset. For the ZooCAM only, the associated images from years 2016 and 2017 contain printed Region Of Interest  
345 (ROI) bounding box limits and text at the bottom of each image, and non-homogenised background within and  
346 around the ROI bounding box; images from year 2018 contain non-homogenised background within the ROI  
347 bounding box only; images from 2019 have a completely homogeneous and thresholded background around the  
348 object. The differences arose from successive ZooCAM software updates that do not modify the calculation of  
349 object's features. The ZooScan images have all a completely homogeneous and thresholded background around  
350 the object, no bounding box limits nor text printed in the images. All images for the two instruments datasets have  
351 a 1 mm scale bar printed at the bottom left corner.

### 352 **4 Data availability**

353 The ZooScan dataset can be found as the *PELGAS Bay of Biscay ZooScan zooplankton Dataset (2004-2016)* in  
354 the SEANOE dataportal following the link: <https://www.seanoe.org/data/00829/94052/> (Grandremy et al., 2023c).  
355 Individual objects images can be freely viewed and explored by anyone using the Ecotaxa ([https://ecotaxa.obs-  
356 vlfr.fr/](https://ecotaxa.obs-vlfr.fr/)) web application, without registration, under the tab “explore images”, by searching the project name:  
357 “*PELGAS Bay of Biscay ZooScan zooplankton Dataset (2004-2016)*”.

358 The ZooCAM dataset can be found as the *PELGAS Bay of Biscay ZooCAM zooplankton Dataset (2016-2019)* in  
359 the SEANOE dataportal <https://www.seanoe.org/data/00828/94040/> (Grandremy et al., 2023d). Individual objects  
360 images can be freely viewed and explored by anyone using the Ecotaxa (<https://ecotaxa.obs-vlfr.fr/>) web  
361 application, without registration, under the tab “explore images”, by searching the project name: “*PELGAS Bay  
362 of Biscay ZooCAM zooplankton Dataset (2016-2019)*”.

363 Each dataset comes as a .zip archive that contains:

- 364 • One tab separated file containing all data and metadata associated to each imaged and identified object.
- 365 • One comma separated file containing the name, type, definition and unit of each field (column)
- 366 • One comma separated file containing the taxonomic list of the dataset, with counts and nature of the  
367 content of the category
- 368 • A directory “*individual\_images*” containing images of each object, named according to the object id  
369 *objid* and sorted in subdirectories according to their taxonomic identification, across years and sampling  
370 stations.

### 371 **5 Concluding remarks**

372 Recent studies showed that the small pelagic fish (SPF) communities have suffered from a drastic  
373 decrease of condition in the Mediterranean Sea and in the Bay of Biscay (Van Beveren et al., 2014; Doray et al.,  
374 2018d; Saraux et al., 2019) over the last 20 years. This loss of condition was especially expressed by the constant  
375 decrease of SPF size- and weight-at-age (Doray et al., 2018d; Veron et al. 2020), and possibly explained by a  
376 change in SPF trophic resource composition, size and quality (Brosset et al., 2016; Queiros et al., 2019; Menu et  
377 al., 2023). Identifying and measuring zooplankton at appropriate temporal and spatial scales is not an easy task,  
378 but can be addressed with imaging. These datasets were assembled as an effort to make possible the exploration

379 of the relationship between SPF observed dynamics in the Bay of Biscay and their main food resource's dynamics,  
380 the metazoan zooplankton. This zooplankton imaging data series is a significant output of Nina Grandremy PhD  
381 (2019-2023), that is currently being exploited (Grandremy et al., 2023a), and is intended to be continued and  
382 updated on a yearly basis in the framework of the PELGAS program, to better understand the underlying processes  
383 presiding to long-term SPF dynamics. Moreover, those two zooplankton datasets can be associated with the  
384 PELGAS survey datasets previously published in 2018, also in the SEANOE dataportal, featuring hydrological,  
385 primary producers, fish and megafauna data arranged as gridded data (Doray et al., 2018b). Together, all these  
386 datasets allow to study simultaneously all the pelagic ecosystem compartments, with coherent spatial domain (the  
387 Bay of Biscay continental shelf), resolution and time series. Nevertheless, a spatial gridding of the data is highly  
388 recommended (as represented in the Fig. 2, 3 and 4), since the spatial coverage of the sampling protocols can vary  
389 between years (Fig. 1), within and between each pelagic ecosystem compartment. A procedure for such batch data  
390 spatial smoothing is presented e.g. in Petitgas et al. (2009) and Petitgas et al. (2014). See also Doray et al. (2018c)  
391 and Grandremy et al. (2023a) for application examples. As several descriptors of the spring zooplankton  
392 community (abundances, sizes, biovolumes, biomass) can be derived from this 16 years long spatially resolved  
393 time series at several taxonomic levels, these datasets are intended to be used in various ecological studies  
394 including the zooplankton compartment, especially modelling studies, where zooplankton is usually  
395 underrepresented (Mitra, 2010; Mitra et al., 2014). Finally, these datasets can also be used for machine learning  
396 applied to plankton studies serving, for example, as consequent learning sets.

### 397 **Disclaimer**

398 Data are published without any warranty, express or implied. The user assumes all risk arising from his/her use of  
399 data. Data are intended to be research-quality, but it is possible that the data themselves contain errors. It is the  
400 sole responsibility of the user to assess if the data are appropriate for his/her use, and to interpret the data  
401 accordingly. Authors welcome users to ask questions and report problems.

### 402 **Authors' contributions**

403 GN scanned and validated most of the ZooScan dataset, assembled the datasets, and led the drafting. BP collected  
404 and managed the samples since 2004, and participated in the manual validation of identifications. DE scanned a  
405 substantial fraction of the ZooScan samples and participated in the initial sorting of vignettes. DMM participated  
406 in the collection of samples, and was involved in the ZooCAM development. DM was chief scientist on the  
407 PELGAS surveys and participated in the drafting. DC supervised GN work and participated in the drafting. FB  
408 developed, improved and maintained the ZooCAM software. JL curated a substantial fraction of the ZooScan  
409 dataset manual validation of identifications. HM participated in the collection of samples, lead the DEFIPEL  
410 project, and participated in the drafting. LMS participated in the collection of samples, and managed the ZooCAM.  
411 NA curated a substantial fraction of the ZooScan and ZooCAM dataset manual validation of identifications. PP  
412 supervised GN work and participated in the drafting. PPh participated in the collection of samples and participated  
413 in the drafting. RJ supervised the development and improvement of the ZooCAM. TM developed and improved  
414 the ZooCAM, and participated in the collection of samples. RJB supervised GN work, participated in the collection  
415 of samples, curated a substantial fraction of the ZooCAM dataset manual validation of identifications, and lead  
416 the drafting.

417 **Competing interests**

418 The authors declare that they have no conflict of interest.

419 **Acknowledgements**

420 The authors acknowledge receiving funding from the ‘France Filière Pêche’ DEFIPEL project. NG acknowledges  
421 the funding of her PhD by Region Pays de la Loire, FR and Ifremer. The authors wish to thank Jean-Yves Coail,  
422 Gérard Guyader and Patrick Berriet (Ifremer – REM-RDT-SIIM) for their contribution to the hardware assembly  
423 of the ZooCAM. The authors acknowledge the work of Elio Raphalen for scanning year 2005 samples. The authors  
424 thank the EMBRC platform PIQs for image analysis. This work was supported by EMBRC-France, whose French  
425 state funds are managed by the ANR within the Investments of the Future program under reference ANR-10-  
426 INBS-02. Finally, the authors wish also to thank the many other students, technicians and scientists who  
427 participated in the sampling and samples imaging on board, and the successive crews of the R/V *Thalassa* involved  
428 in the PELGAS surveys from 2004 to 2019.

429

430 **References**

- 431 Ahlstrom, E.H., 1943. Studies on the Pacific Pilchard Or Sardine (*Sardinops Caerulea*): Influence of Temperature  
432 on the Rate of Development of Pilchard Eggs in Nature. United States Department of the Interior, Fish and Wildlife  
433 Service.
- 434 Banse, K., 1995. Zooplankton: Pivotal role in the control of ocean production: I. Biomass and production. ICES  
435 Journal of Marine Science 52, 265–277. [https://doi.org/10.1016/1054-3139\(95\)80043-3](https://doi.org/10.1016/1054-3139(95)80043-3)
- 436 Batten, S.D., Abu-Alhaja, R., Chiba, S., Edwards, M., Graham, G., Jyothibabu, R., Kitchener, J.A., Koubbi, P.,  
437 McQuatters-Gollop, A., Muxagata, E., Ostle, C., Richardson, A.J., Robinson, K.V., Takahashi, K.T., Verheye,  
438 H.M., Wilson, W., 2019. A Global Plankton Diversity Monitoring Program. *Frontiers in Marine Science* 6.  
439 <https://doi.org/10.3389/fmars.2019.00321>
- 440 Beaugrand, G., Brander, K.M., Lindley, J.A., Souissi, S., Reid, P.C., 2003. Plankton effect on cod recruitment in  
441 the North Sea. *Nature* 426, 661–664. <https://doi.org/10.1038/nature02164>
- 442 Benedetti, F., Jalabert, L., Sourisseau, M., Becker, B., Cailliau, C., Desnos, C., Elineau, A., Irisson, J.-O.,  
443 Lombard, F., Picheral, M., Stemmann, L., Pouline, P., 2019. The Seasonal and Inter-Annual Fluctuations of  
444 Plankton Abundance and Community Structure in a North Atlantic Marine Protected Area. *Front. Mar. Sci.* 6.  
445 <https://doi.org/10.3389/fmars.2019.00214>
- 446 Biard, T., Stemmann, L., Picheral, M., Mayot, N., Vandromme, P., Hauss, H., Gorsky, G., Guidi, L., Kiko, R.,  
447 Not, F., 2016. In situ imaging reveals the biomass of giant protists in the global ocean. *Nature* 532, 504–507.  
448 <https://doi.org/10.1038/nature17652>
- 449 Breiman, L., 2001. Random forests. *Mach. Learn.* 45, 5–32. <https://doi.org/10.1023/A:1010933404324>

450 Brosset, P., Le Bourg, B., Costalago, D., Banaru, D., Van Beveren, E., Bourdeix, J.-H., Fromentin, J.-M., Menard,  
451 F., Saraux, C., 2016. Linking small pelagic dietary shifts with ecosystem changes in the Gulf of Lions. *Mar. Ecol.-*  
452 *Prog. Ser.* 554, 157–171. <https://doi.org/10.3354/meps11796>

453 Chiba, S., Batten, S., Martin, C.S., Ivory, S., Miloslavich, P., Weatherdon, L.V., 2018. Zooplankton monitoring to  
454 contribute towards addressing global biodiversity conservation challenges. *Journal of Plankton Research* 40, 509–  
455 518. <https://doi.org/10.1093/plankt/fby030>

456 Colas, F., Tardivel, M., Perchoc, J., Lunven, M., Forest, B., Guyader, G., Danielou, M.M., Le Mestre, S., Bourriau,  
457 P., Antajan, E., Sourisseau, M., Huret, M., Petitgas, P., Romagnan, J.B., 2018. The ZooCAM, a new in-flow  
458 imaging system for fast onboard counting, sizing and classification of fish eggs and metazooplankton. *Progress in*  
459 *Oceanography, Multidisciplinary integrated surveys* 166, 54–65. <https://doi.org/10.1016/j.pocean.2017.10.014>

460 Culverhouse, P.F., 2007. Human and machine factors in algae monitoring performance. *Ecol. Inform.* 2, 361–366.  
461 <https://doi.org/10.1016/j.ecoinf.2007.07.001>

462 Cury, P., Bakun, A., Crawford, R.J.M., Jarre, A., Quiñones, R.A., Shannon, L.J., Verheye, H.M., 2000. Small  
463 pelagics in upwelling systems: patterns of interaction and structural changes in “wasp-waist” ecosystems. *ICES*  
464 *Journal of Marine Science* 57, 603–618. <https://doi.org/10.1006/jmsc.2000.0712>

465 Doray, M., Boyra, G., van der Kooij, J., 2021. ICES Survey Protocols - Manual for acoustic surveys coordinated  
466 under ICES Working Group on Acoustic and Egg Surveys for Small Pelagic Fish (WGACEGG).  
467 <https://doi.org/10.17895/ICES.PUB.7462>

468 Doray, M., Petitgas, P., Romagnan, J.B., Huret, M., Duhamel, E., Dupuy, C., Spitz, J., Authier, M., Sanchez, F.,  
469 Berger, L., Dorémus, G., Bourriau, P., Grellier, P., Massé, J., 2018a. The PELGAS survey: Ship-based integrated  
470 monitoring of the Bay of Biscay pelagic ecosystem. *Progress in Oceanography, Multidisciplinary integrated*  
471 *surveys* 166, 15–29. <https://doi.org/10.1016/j.pocean.2017.09.015>

472 Doray, M., Huret, M., Authier, M., Duhamel, E., Romagnan, J.-B., Dupuy, C., Spitz, J., Sanchez, F., Berger, L.,  
473 Dorémus, G., Bourriau, P., Grellier, P., Pennors, L., Masse, J., Petitgas, P., 2018b. Gridded maps of pelagic  
474 ecosystem parameters collected in the Bay of Biscay during the PELGAS integrated survey.  
475 <https://doi.org/10.17882/53389>

476 Doray, M., Hervy, C., Huret, M., Petitgas, P., 2018c. Spring habitats of small pelagic fish communities in the Bay  
477 of Biscay. *Progress in Oceanography, Multidisciplinary integrated surveys* 166, 88–108.  
478 <https://doi.org/10.1016/j.pocean.2017.11.003>

479 Doray, M., Petitgas, P., Huret, M., Duhamel, E., Romagnan, J.B., Authier, M., Dupuy, C., Spitz, J., 2018d.  
480 Monitoring small pelagic fish in the Bay of Biscay ecosystem, using indicators from an integrated survey. *Progress*  
481 *in Oceanography* 166, 168–188. <https://doi.org/10.1016/j.pocean.2017.12.004>

482 Elineau, A., Desnos, C., Jalabert, L., Olivier, M., Romagnan, J.-B., Costa Brandao, M., Lombard, F., Llopis, N.,  
483 Courboulès, J., Caray-Counil, L., Serranito, B., Irisson, J.-O., Picheral, M., Gorsky, G., Stemann, L., 2018.  
484 ZooScanNet: plankton images captured with the ZooScan. <https://doi.org/10.17882/55741>

485 Feuilletoy, G., Fromentin, J.-M., Saraux, C., Irisson, J.-O., Jalabert, L., Stemmann, L., 2022. Temporal fluctuations  
486 in zooplankton size, abundance, and taxonomic composition since 1995 in the North Western Mediterranean Sea.  
487 ICES J. Mar. Sci. 79, 882–900. <https://doi.org/10.1093/icesjms/fsab190>

488 Gorsky, G., Ohman, M.D., Picheral, M., Gasparini, S., Stemmann, L., Romagnan, J.-B., Cawood, A., Pesant, S.,  
489 Garcia-Comas, C., Prejger, F., 2010. Digital zooplankton image analysis using the ZooScan integrated system. J.  
490 Plankton Res. 32, 285–303. <https://doi.org/10.1093/plankt/fbp124>

491 Graham, B., 2014. Spatially-sparse convolutional neural networks. <https://doi.org/10.48550/arXiv.1409.6070>

492 Grandremy, N., Romagnan, J.-B., Dupuy, C., Doray, M., Huret, M., Petitgas, P., 2023a. Hydrology and small  
493 pelagic fish drive the spatio-temporal dynamics of springtime zooplankton assemblages over the Bay of Biscay  
494 continental shelf. Progress in Oceanography 210, 102949. <https://doi.org/10.1016/j.pocean.2022.102949>

495 [Grandremy, N., Dupuy, C., Petitgas, P., Mestre, S.L., Bourriau, P., Nowaczyk, A., Forest, B., Romagnan, J.-B.,  
496 2023b. The ZooScan and the ZooCAM zooplankton imaging systems are intercomparable: A benchmark on the  
497 Bay of Biscay zooplankton. Limnology and Oceanography: Methods 21, 718–733.  
498 <https://doi.org/10.1002/lom3.10577>](https://doi.org/10.1002/lom3.10577)

499 Grandremy N., Bourriau P., Daché E., Danielou M-M., Doray M., Dupuy C., Huret M., Jalabert L., Le Mestre S.,  
500 Nowaczyk A., Petitgas P., Pineau P., Raphalen E., Romagnan J-B., 2023c. PELGAS Bay of Biscay ZooScan  
501 zooplankton Dataset (2004-2016). SEANO. <https://doi.org/10.17882/94052>

502 Grandremy N., Bourriau P., Danielou M-M., Doray M., Dupuy C., Forest B., Huret M., Le Mestre S., Nowaczyk  
503 A., Petitgas P., Pineau P., Rouxel J., Tardivel M., Romagnan J-B., 2023d. PELGAS Bay of Biscay ZooCAM  
504 zooplankton Dataset (2016-2019). SEANO. <https://doi.org/10.17882/94040>

505 ICES, 2021. Bay of Biscay and Iberian Coast ecoregion – Fisheries overview (report). ICES Advice: Fisheries  
506 Overviews. <https://doi.org/10.17895/ices.advice.9100>

507 Irisson, J.-O., Ayata, S.-D., Lindsay, D.J., Karp-Boss, L., Stemmann, L., 2022. Machine Learning for the Study of  
508 Plankton and Marine Snow from Images. Annual Review of Marine Science 14, 277–301.  
509 <https://doi.org/10.1146/annurev-marine-041921-013023>

510 Lombard, F., Boss, E., Waite, A.M., Vogt, M., Uitz, J., Stemmann, L., Sosik, H.M., Schulz, J., Romagnan, J.-B.,  
511 Picheral, M., Pearlmann, J., Ohman, M.D., Niehoff, B., Möller, K.O., Miloslavich, P., Lara-Lpez, A., Kudela, R.,  
512 Lopes, R.M., Kiko, R., Karp-Boss, L., Jaffe, J.S., Iversen, M.H., Irisson, J.-O., Fennel, K., Hauss, H., Guidi, L.,  
513 Gorsky, G., Giering, S.L.C., Gaube, P., Gallager, S., Dubelaar, G., Cowen, R.K., Carlotti, F., Briseño-Avena, C.,  
514 Berline, L., Benoit-Bird, K., Bax, N., Batten, S., Ayata, S.D., Artigas, L.F., Appeltans, W., 2019. Globally  
515 Consistent Quantitative Observations of Planktonic Ecosystems. Front. Mar. Sci. 6.  
516 <https://doi.org/10.3389/fmars.2019.00196>

517 Menu, C., Pecquerie, L., Bacher, C., Doray, M., Hattab, T., van der Kooij, J., Huret, M., 2023. Testing the bottom-  
518 up hypothesis for the decline in size of anchovy and sardine across European waters through a bioenergetic  
519 modeling approach. Progress in Oceanography 210, 102943. <https://doi.org/10.1016/j.pocean.2022.102943>

520 Mitra, A., Castellani, C., Gentleman, W.C., Jonasdottir, S.H., Flynn, K.J., Bode, A., Halsband, C., Kuhn, P.,  
521 Licandro, P., Agersted, M.D., Calbet, A., Lindeque, P.K., Koppelman, R., Moller, E.F., Gislason, A., Nielsen,  
522 T.G., John, M.S., 2014. Bridging the gap between marine biogeochemical and fisheries sciences; configuring the  
523 zooplankton link. *Prog. Oceanogr.* 129, 176–199. <https://doi.org/10.1016/j.pocean.2014.04.025>

524 Mitra, A., Davis, C., 2010. Defining the “to” in end-to-end models. *Prog. Oceanogr.* 84, 39–42.  
525 <https://doi.org/10.1016/j.pocean.2009.09.004>

526 Moser, H.G., Ahlstrom, E.H., 1985. Staging anchovy eggs. Southwest Fisheries Center, National Marine Fisheries  
527 Service, NOM, PO. Box 271, La Jolla, CA 92038.

528 Ohman, M.D., Romagnan, J.-B., 2016. Nonlinear effects of body size and optical attenuation on Diel Vertical  
529 Migration by zooplankton. *Limnology and Oceanography* 61, 765–770. <https://doi.org/10.1002/lno.10251>

530 Orenstein, E.C., Ayata, S.-D., Maps, F., Becker, É.C., Benedetti, F., Biard, T., de Garidel-Thoron, T., Ellen, J.S.,  
531 Ferrario, F., Giering, S.L.C., Guy-Haim, T., Hoebeke, L., Iversen, M.H., Kiørboe, T., Lalonde, J.-F., Lana, A.,  
532 Laviale, M., Lombard, F., Lorimer, T., Martini, S., Meyer, A., Möller, K.O., Niehoff, B., Ohman, M.D., Pradalié,  
533 C., Romagnan, J.-B., Schröder, S.-M., Sonnet, V., Sosik, H.M., Stemmann, L.S., Stock, M., Terbiyik-Kurt, T.,  
534 Valcárcel-Pérez, N., Vilgrain, L., Wacquet, G., Waite, A.M., Irisson, J.-O., 2022. Machine learning techniques to  
535 characterize functional traits of plankton from image data. *Limnology and Oceanography* 67, 1647–1669.  
536 <https://doi.org/10.1002/lno.12101>

537 Panaiotis, T., Caray-Counil, L., Woodward, B., Schmid, M.S., Daprano, D., Tsai, S.T., Sullivan, C.M., Cowen,  
538 R.K., Irisson, J.-O., 2022. Content-Aware Segmentation of Objects Spanning a Large Size Range: Application to  
539 Plankton Images. *Frontiers in Marine Science* 9.

540 Petitgas, P., Goarant, A., Masse, J., and Bourriau, P., 2009. Combining acoustic and CUFES data for the quality  
541 control of fish-stock survey estimates. *ICES Journal of Marine Science*, 66: 1384–1390.  
542 <https://doi.org/10.1093/icesjms/fsp007>

543 Petitgas, P., Doray, M., Huret, M., Masse, J., and Woillez, M., 2014. Modelling the variability in fish spatial  
544 distributions over time with empirical orthogonal functions: anchovy in the Bay of Biscay. *ICES Journal of Marine  
545 Science*, 71: 2379–2389. <https://doi.org/10.1093/icesjms/fsu111>

546 Picheral, M., Colin, S., Irisson, J.O., 2017. EcoTaxa, a tool for the taxonomic classification of images. URL  
547 <https://ecotaxa.obs-vlfr.fr/>

548 Queiros, Q., Fromentin, J.-M., Gasset, E., Dutto, G., Huiban, C., Metral, L., Leclerc, L., Schull, Q., McKenzie,  
549 D.J., Saraux, C., 2019. Food in the Sea: Size Also Matters for Pelagic Fish. *Frontiers in Marine Science* 6.  
550 <https://doi.org/10.3389/fmars.2019.00385>

551 Romagnan, J.B., Aldamman, L., Gasparini, S., Nival, P., Aubert, A., Jamet, J.L., Stemmann, L., 2016. High  
552 frequency mesozooplankton monitoring: Can imaging systems and automated sample analysis help us describe  
553 and interpret changes in zooplankton community composition and size structure - An example from a coastal site.  
554 *Journal of Marine Systems* 162, 18–28. <https://doi.org/10.1016/j.jmarsys.2016.03.013>

555 Saraux, C., Beveren, E.V., Brosset, P., Queiros, Q., Bourdeix, J.-H., Dutto, G., Gasset, E., Jac, C., Bonhommeau,  
556 S., Fromentin, J.-M., 2019. Small pelagic fish dynamics: A review of mechanisms in the Gulf of Lions. *Deep Sea*  
557 *Research Part II: Topical Studies in Oceanography* 159, 52–61. <https://doi.org/10.1016/j.dsr2.2018.02.010>

558 Sieburth, J., Smetacek, V., Lenz, J., 1978. Pelagic Ecosystem Structure - Heterotrophic Compartments of Plankton  
559 and Their Relationship to Plankton Size Fractions - Comment. *Limnol. Oceanogr.* 23, 1256–1263.  
560 <https://doi.org/10.4319/lo.1978.23.6.1256>

561 Siegel, D.A., Buesseler, K.O., Behrenfeld, M.J., Benitez-Nelson, C.R., Boss, E., Brzezinski, M.A., Burd, A.,  
562 Carlson, C.A., D'Asaro, E.A., Doney, S.C., Perry, M.J., Stanley, R.H.R., Steinberg, D.K., 2016. Prediction of the  
563 Export and Fate of Global Ocean Net Primary Production: The EXPORTS Science Plan. *Frontiers in Marine*  
564 *Science* 3. <https://doi.org/10.3389/fmars.2016.00022>

565 Steinberg, D.K., Carlson, C.A., Bates, N.R., Goldthwait, S.A., Madin, L.P., Michaels, A.F., 2000. Zooplankton  
566 vertical migration and the active transport of dissolved organic and inorganic carbon in the Sargasso Sea. *Deep*  
567 *Sea Research Part I: Oceanographic Research Papers* 47, 137–158. [https://doi.org/10.1016/S0967-0637\(99\)00052-](https://doi.org/10.1016/S0967-0637(99)00052-7)  
568 [7](https://doi.org/10.1016/S0967-0637(99)00052-7)

569 Turner, J.T., 2015. Zooplankton fecal pellets, marine snow, phytodetritus and the ocean's biological pump.  
570 *Progress in Oceanography* 130, 205–248. <https://doi.org/10.1016/j.pocean.2014.08.005>

571 Uitz, J., Claustre, H., Gentili, B., Stramski, D., 2010. Phytoplankton class-specific primary production in the  
572 world's oceans: Seasonal and interannual variability from satellite observations. *Global Biogeochemical Cycles*  
573 24. <https://doi.org/10.1029/2009GB003680>

574 Van Beveren, E., Bonhommeau, S., Fromentin, J.-M., Bigot, J.-L., Bourdeix, J.-H., Brosset, P., Roos, D., Saraux,  
575 C., 2014. Rapid changes in growth, condition, size and age of small pelagic fish in the Mediterranean. *Mar Biol*  
576 161, 1809–1822. <https://doi.org/10.1007/s00227-014-2463-1>

577 van der Lingen, C., Hutchings, L., Field, J., 2006. Comparative trophodynamics of anchovy *Engraulis encrasicolus*  
578 and sardine *Sardinops sagax* in the southern Benguela: are species alternations between small pelagic fish  
579 trophodynamically mediated? *African Journal of Marine Science* 28, 465–477.  
580 <https://doi.org/10.2989/18142320609504199>

581 Vandromme, P., Nogueira, E., Huret, M., Lopez-Urrutia, A., Gonzalez-Nuevo Gonzalez, G., Sourisseau, M.,  
582 Petitgas, P., 2014. Springtime zooplankton size structure over the continental shelf of the Bay of Biscay. *Ocean*  
583 *Sci.* 10, 821–835. <https://doi.org/10.5194/os-10-821-2014>

584 Vandromme, P., Stemmann, L., Garcia-Comas, C., Berline, L., Sun, X., Gorsky, G., 2012. Assessing biases in  
585 computing size spectra of automatically classified zooplankton from imaging systems: A case study with the  
586 ZooScan integrated system. *Methods in Oceanography* 1–2, 3–21. <https://doi.org/10.1016/j.mio.2012.06.001>

587 Véron, M., Duhamel, E., Bertignac, M., Pawlowski, L., Huret, M., 2020. Major changes in sardine growth and  
588 body condition in the Bay of Biscay between 2003 and 2016: Temporal trends and drivers. *Progress in*  
589 *Oceanography* 182, 102274. <https://doi.org/10.1016/j.pocean.2020.102274>





591 **Appendix A**

592 Table A1: ZooCAM dataset columns header – definition of data and metadata fields.

column name	definition
object_id	name of object and associated image
objid	unique ecotaxa internal object identifier
object_lat	latitude of sampling
object_lon	longitude of sampling
object_date	date of sampling
object_time	time of sampling
object_depth_min	minimum sampling depth
object_depth_max	maximum sampling depth
object_taxon	taxonomic name
object_lineage	full taxonomic lineage corresponding to the taxon
classif_id	unique ecotaxa internal taxon identifier
object_area	object's surface
object_area_exc	object surface excluding white pixels
object_%area	proportion of the image corresponding to the object
object_area_based_diameter	object's Area Based Diameter: $2 * (\text{object\_area}/\pi)^{(1/2)}$
object_meangreyimage	mean image grey level
object_meangreyobject	mean object grey level
object_modegreyobject	modal object grey level
object_sigmagrey	object grey level standard deviation
object_mingrey	minimum object grey level
object_maxgrey	maximum object grey level
object_sumgrey	object grey level integrated density: $\text{object\_mean} * \text{object\_area}$
object_breadth	breadth of the object along the best fitting ellipsoid minor axis
object_length	breadth of the object along the best fitting ellipsoid major axis
object_elongation	elongation index: $\text{object\_length}/\text{object\_breadth}$
object_perim	object's perimeter
object_minferetdiam	minimum object's feret diameter
object_maxferetdiam	maximum object's feret diameter
object_meanferetdiam	average object's feret diameter
object_feretelongation	elongation index: $\text{object\_maxferetdiam}/\text{object\_minferetdiam}$
object_compactness	Isoperimetric quotient: the ratio of the object's area to the area of a circle having the same perimeter
object_intercept0	number of times that a transition from background to foreground occurs at the angle 0° for the entire object
object_intercept45	the number of times that a transition from background to foreground occurs at the angle 45° for the entire object
object_intercept90	the number of times that a transition from background to foreground occurs at the angle 90° for the entire object
object_intercept135	the number of times that a transition from background to foreground occurs at the angle 135° for the entire object
object_convexhullarea	area of the convex hull of the object
object_convexhullfillratio	ratio $\text{object\_area}/\text{convexhullarea}$
object_convexperimeter	perimeter of the convex hull of the object
object_n_number_of_runs	number of horizontal strings of consecutive foreground pixels in the object
object_n_chained_pixels	number of chained pixels in the object
object_n_convex_hull_points	number of summits of the object's convex hull polygon
object_n_number_of_holes	number of holes (as closed white pixel area) in the object
object_transparence	ratio $\text{object\_sumgrey}/\text{object\_area}$
object_roughness	measure of small scale variations of amplitude in the object's grey levels
object_rectangularity	ratio of the object's area over its best bounding rectangle's area
object_skewness	skewness of the object's grey level distribution
object_kurtosis	kurtosis of the object's grey level distribution
object_fractal_box	fractal dimension of the object's perimeter
object_hist25	grey level value at quantile 0.25 of the object's grey levels normalized cumulative histogram
object_hist50	grey level value at quantile 0.5 of the object's grey levels normalized cumulative histogram
object_hist75	grey level value at quantile 0.75 of the object's grey levels normalized cumulative histogram
object_valhist25	sum of grey levels at quantile 0.25 of the object's grey levels normalized cumulative histogram
object_valhist50	sum of grey levels at quantile 0.5 of the object's grey levels normalized cumulative histogram
object_valhist75	sum of grey levels at quantile 0.75 of the object's grey levels normalized cumulative histogram
object_nobj25	number of objects after thresholding at the object_valhist25 grey level
object_nobj50	number of objects after thresholding at the object_valhist50 grey level
object_nobj75	number of objects after thresholding at the object_valhist75 grey level
object_symetrieh	index of horizontal symmetry
object_symetriev	index of vertical symmetry
object_thick_r	maximum object's thickness/mean object's thickness
object_cdist	distance between the mass and the grey level object's centroids
object_bord	tag for object touching the frame edge
sample_id	name of the sample from where the object originates
sample_ship	name of the ship used to collect the samples
sample_campaign	name of the cruise where samples were collected
sample_station	name of the station where samples were collected
sample_depth	bottom depth at station
sample_device	net used to collect the sample
sample_fishingvolume	seawater volume sampled
sample_sub_part	subsampling elevation factor
process_id	name of software/software version used to analyse digitized sample images
process_resolution_camera_micron	pixel size, $\mu\text{m}$

593

594 Table A2: ZooScan dataset columns header – definition of data and metadata fields

column name	definition
object_id	name of object and associated image
objid	unique ecotaxa internal object identifier
object_lat	latitude of sampling
object_lon	longitude of sampling
object_date	date of sampling
object_time	time of sampling
object_depth_min	minimum sampling depth
object_depth_max	maximum sampling depth
object_taxon	taxonomic name
object_lineage	full taxonomic lineage corresponding to the taxon
classif_id	unique ecotaxa internal taxon identifier
object_area	object's surface
object_mean	mean object grey level
object_stddev	object grey level standard deviation
object_mode	modal object grey level
object_min	minimum object grey level
object_max	maximum object grey level
object_perim.	object's perimeter
object_major	length of major axis of best fitting ellipse
object_minor	length of minor axis of best fitting ellipse
object_circ.	circularity: $4 * \pi * (\text{object\_area} / \text{object\_perim.}^2)$
object_feret	maximum feret diameter
object_intden	object grey level integrated density: $\text{object\_mean} * \text{object\_area}$
object_median	median object grey level
object_skew	skewness of the object's grey level distribution
object_kurt	kurtosis of the object's grey level distribution
object_%area	proportion of the image corresponding to the object
object_area_exc	object surface excluding white pixels
object_fractal	fractal dimension of the object's perimeter
object_skelarea	surface of the one-pixel wide skeleton of the object
object_slope	slope of the cumulated histogram of the object grey levels
object_histcum1	the number of times that a transition from background to foreground occurs at the angle $0^\circ$
object_histcum2	grey level at quantiles 0.5 of the histogram of the object grey levels
object_histcum3	grey level at quantiles 0.75 of the histogram of the object grey levels
object_nb1	number of objects after thresholding at the object_histcum1 grey level
object_nb2	number of objects after thresholding at the object_histcum2 grey level
object_symetrieh	index of horizontal symmetry
object_symetriev	index of vertical symmetry
object_symetriehc	index of horizontal symmetry after thresholding at the object_histcum1 grey level
object_symetrievc	index of vertical symmetry after thresholding at the object_histcum1 grey level
object_convperim	perimeter of the convex hull of the object
object_convarea	area of the convex hull of the object
object_fcons	object's contrast
object_thickr	maximum object's thickness/mean object's thickness
object_esd	object's Equivalent Spherical Diameter: $2 * (\text{object\_area} / \pi)^{1/2}$
object_elongation	elongation index: major/minor
object_range	range of greys: max-min
object_meanpos	relative position of the mean grey: $(\text{max} - \text{mean}) / \text{range}$
object_centroids	distance between the mass and the grey level object's centroids
object_cv	coefficient of variation of greys: $100 * (\text{stddev} / \text{mean})$
object_sr	index of variation of greys: $100 * (\text{stddev} / \text{range})$
object_perimareaexc	index of the relative complexity of the perimeter: $\text{object\_perim} / \text{object\_area\_exc}$
object_feretareaexc	another elongation index : $\text{object\_feret} / \text{object\_area\_exc}$
object_perimferet	index of the relative complexity of the perimeter: $\text{object\_perim} / \text{object\_feret}$
object_perimmajor	index of the relative complexity of the perimeter: $\text{object\_perim} / \text{object\_major}$
object_circexc	circularity of object excluding white pixels: $4 * \pi * (\text{object\_area\_exc} / \text{object\_perim.}^2)$
object_cdexc	distance between the mass and the grey level object's centroids calculated with object_area_exc
sample_id	name of the sample from the object originate
sample_ship	name of the ship used to collect the samples
sample_program	name of the cruise where samples were collected
sample_stationid	name of the station where samples were collected
sample_bottomdepth	bottom depth at station
sample_net_type	net used to collect the sample
sample_tot_vol	seawater volume sampled
sample_comment	comments associated with sampling/sample treatment
process_id	name of software/software version used to analysed digitized sample images
process_particle_pixel_size_mm	pixel size
acq_id	name of subsample if any
acq_min_mesh	minimum sieve size of subsample
acq_max_mesh	maximum sieve size of subsample
acq_sub_part	subsampling elevation factor

595

596